

## Production of Hadrons with Large Transverse Momentum at 200 and 300 GeV\*

J. W. Cronin, H. J. Frisch, and M. J. Shochet

The Enrico Fermi Institute, University of Chicago, Chicago, Illinois 60637

and

J. P. Boymond, P. A. Piroué, and R. L. Sumner

Department of Physics, Joseph Henry Laboratories

Princeton University, Princeton, New Jersey 08540

## ABSTRACT

Differential cross sections as a function of transverse momentum are presented for the production at  $\sim 90^\circ$  c.m. of  $\pi^\pm$ ,  $K^\pm$ ,  $p$ , and  $\bar{p}$  in  $p$ -nucleus collisions at incident proton energies of 200 and 300 GeV.

Investigations of large transverse momentum ( $p_\perp$ ) phenomena are interesting because of their possible relation to basic processes at small distances. Experimentally, it had been known<sup>1</sup> for some time that the  $p_\perp$  distributions of long-lived particles produced in high-energy hadron collisions were falling off exponentially ( $e^{-bp_\perp}$ ), with the average transverse momentum  $\langle p_\perp \rangle = 0.3 - 0.5$  GeV/c, independent both of the secondary particle energy  $E$  and of the c.m. energy  $\sqrt{s}$  of the collision. Recent measurements<sup>2</sup> at the CERN Intersecting Storage Rings (ISR) have in general confirmed these  $\langle p_\perp \rangle$  values. However, at high  $p_\perp$  ( $> 3$  GeV/c), a much more copious pion production has been observed<sup>3,4,5</sup> than predicted by the extrapolation of the data at small  $p_\perp$  ( $< 1$  GeV/c).

In an experiment at the National Accelerator Laboratory (NAL) we have measured, as a function of  $p_{\perp}$ , the invariant cross section  $E d\sigma/d^3p$  for the production of  $\pi^{\pm}$ ,  $K^{\pm}$ ,  $p$ , and  $\bar{p}$  in p-nucleus collisions at incident proton energies of 200 and 300 GeV. The measurements were made in the region of  $90^{\circ}$  in the c.m. system of the incident proton and a single nucleon at rest.

Figure 1 shows a schematic view of the apparatus. The NAL proton beam, extracted from the main ring and transported  $\sim 1.1$  miles away to the target box of the Proton East Laboratory, impinged on a 2-in.-long, 1/8-in.-diam tungsten target. Particles emitted at 77 mrad ( $\sim 90^{\circ}$  in the proton-nucleon c.m.) relative to the direction of the incident proton beam traversed a  $\sim 330$  ft.-long magnetic spectrometer consisting of a quadrupole doublet, 2 collimators, 2 bending magnets, and 4 scintillation hodoscopes  $H_1 - H_4$ . The momentum acceptance was 10% with a solid angle  $\Delta\Omega = 17 \mu\text{sr}$ . Each hodoscope consisted of a 4-in.-wide, 2-in.-high, 1/4-in.-thick trigger counter (A) followed by an array of 5 horizontal and 17 vertical 1/8-in.-thick scintillator channels. This arrangement allowed us to determine the momentum of individual events to within  $\pm 1\%$ , and to reconstruct the position of each track at the target to within  $\pm 0.4$  in. horizontally, and  $\pm 0.08$  in. vertically. This check was essential at high momentum to eliminate background.

Particles were identified in the Cerenkov counter located between  $H_3$  and  $H_4$ . It was a 80-ft.-long, 1-ft.-diam stainless steel tube with non-reflecting walls, bolted to a 6-ft.-long, 2-ft.-diam optical section in which the Cerenkov light was split into 2 channels (0 - 9 and 9 - 38 mrad), and focussed on 2-in. photomultipliers (RCA 31000 M). Depending on the momentum and the particle type the counter was filled either with He or  $\text{CO}_2$  at pressures ranging from  $\sim 0$  to 10 atm.

A charged particle was signalled by the coincidence  $A_1A_2A_3A_4$ . Information from the counters was fed to a PDP-9 computer. The hodoscope information was used to reconstruct particle tracks through the spectrometer back to the target.

The proton beam striking the target was monitored by 2 three-counter telescopes located at  $90^\circ$  relative to the direction of the incident proton beam and directed at the target. The absolute calibration of the monitors against the proton beam intensity was done in two ways (radiochemical and ion chamber). However, while the relative accuracy of the monitors was better than 5% their absolute calibration was estimated to be known only to  $\sim 50\%$ .

We measured the particle yields at laboratory momenta ranging from 10 to 100 GeV/c, corresponding to  $p_\perp = 0.76$  to 7.6 GeV/c. In order to handle the high counting rates encountered below 40 GeV/c smaller trigger counters were used and the hodoscopes removed. Accidental coincidences, monitored continuously, were found to be negligible except at high momenta ( $> 70$  GeV/c) where the requirement that the observed events originated in the target was essential in the elimination of this background. The data were corrected for nuclear absorption and multiple Coulomb scattering in the apparatus (significant only below 20 GeV/c), and, when appropriate, for particle decay.

The particle yields were converted into equivalent cross sections in p-nucleon collisions by using the following formula:

$$Ed\sigma/d^3p = \sigma_p (\text{yield/incident proton})/p^2 (\Delta\Omega\Delta p/p)f,$$

where  $p$  denotes the laboratory momentum,  $\sigma_p$  the proton-nucleon total cross section which we took to be 40 mb, and  $f$  is the fraction of incident protons interacting in the target. Using an absorption cross section in  $W$  of 1635 mb

one obtains, for a 2-in. target,  $f = 0.41$ . The quantity  $\Delta\Omega\Delta p/p = 1.7 \times 10^{-6}$ , the spectrometer acceptance, was calculated by Monte-Carlo techniques.

The production cross sections for  $\pi^\pm$ , and those for  $K^\pm$ ,  $p$ , and  $\bar{p}$  relative to pions of the same charge, are listed as a function of  $p_\perp$ , in Table I. In Fig. 2 we have plotted, as an illustration, the  $\pi^-$  cross section against  $p_\perp$  at both incident proton energies. (The  $\pi^+$  cross section has similar behavior.) We observe a fall-off with  $p_\perp$  which is slower than exponential, and an energy dependence which, though very small at low  $p_\perp$ , becomes stronger as  $p_\perp$  increases. This is in qualitative agreement with the work of the Saclay-Strasbourg group<sup>3</sup>, and of the CERN-Columbia-Rockefeller group<sup>4</sup> at the ISR.

Most of the theoretical models<sup>6</sup> which have been proposed predict for the single pion inclusive cross section at  $\sim 90^\circ$  c.m. a behavior, at high  $p_\perp$ , of the form  $g(s)f(x_\perp)$ , where  $g(s)$  is some function (generally a power law) of  $s$ , the square of the c.m. energy of the collision, and  $f(x_\perp)$  is a function of the scaling variable  $x_\perp = 2p_\perp/\sqrt{s}$ . If our pion data can indeed be expressed in such a form, then the logarithm of the cross section plotted against  $x_\perp$  at both c.m. energies (19.4 and 23.8 GeV) should yield parallel curves, independent of the absolute calibration. Figure 3 shows that this is approximately so only at large  $x_\perp$  ( $> 0.4$ ) where, for example, the form  $s^{-5.4}\exp(-36x_\perp)$  is found to give a good representation of our data. At low  $x_\perp$  ( $< 0.3$ ), however, the curves become slowly steeper as  $\sqrt{s}$  increases (the higher energy curves are the ISR  $\pi^0$  data<sup>4</sup>).

The  $K^\pm$ ,  $p$  and  $\bar{p}$  yields relative to pions are displayed as functions of  $x_\perp$  in Fig. 4. With the exception of  $p/\pi^+$  the ratios do not change dramatically with incident proton energy. In fact for  $x_\perp > 0.4$  the ratios are, to a good approximation, independent of energy. For  $p_\perp > 3.0$  GeV/c the ratios of heavy particles ( $K^\pm$ ,  $p$ ,  $\bar{p}$ ) to pions do not increase with  $p_\perp$  as sug-

gested by measurements at the ISR at lower  $p_{\perp}^5$ . As  $x_{\perp}$  is increased from 0.2 to 0.5 the ratios  $K^-/K^+$  and  $\bar{p}/p$  decrease by a factor of  $\sim 2$  and  $\sim 4$ , respectively. This is a feature qualitatively similar to that found in hadron production at small  $x_{\perp}$  and large  $x = 2p_{\parallel}/\sqrt{s}$ .

Finally it should be mentioned that auxiliary measurements made with beryllium and titanium targets established that none of the important features observed in tungsten were dependent on atomic number.

We wish to express our appreciation to the staffs of NAL and especially of the Proton Area who have contributed enormous time and effort to make this experiment possible. We are also indebted to K. Wright for the excellent performance of the Cerenkov counter.

REFERENCES

\*Work supported by the National Science Foundation and the U.S. Atomic Energy Commission.

1. See, for example, G. Cocconi, Nuovo Cimento 57 A, 837 (1968).
2. A. Bertin et al., Phys. Letters 42 B, 493 (1972); M. Banner et al., Phys. Letters 41 B, 547 (1972).
3. M. Banner et al., Phys. Letters 44 B, 537 (1973).
4. F. W. Büsser et al., CERN preprint (10 August 1973), to be published in Phys. Letters.
5. B. Alper et al., Phys. Letters 44 B, 521 and 527 (1973).
6. See, for example, S. M. Berman, J. D. Bjorken, and J. B. Kogut, Phys. Rev. D4, 3388 (1971); R. Blankenbecler, S. J. Brodsky, and J. F. Gunion, Phys. Letters 42 B, 461 (1972); P. V. Landshoff and J. C. Polkinghorne, Phys. Letters 45 B, 361 (1973); S. D. Ellis and M. B. Kislinger, NAL preprint Pub-73/40/THY, to be published in Phys. Rev.

FIGURE CAPTIONS

- Fig. 1. Experimental arrangement
- Fig. 2. Transverse momentum distribution of  $\pi^-$  mesons produced at  $\sim 90^\circ$  c.m. in p-W collisions at incident proton energies of 200 and 300 GeV.
- Fig. 3. The average of the  $\pi^+$  and  $\pi^-$  invariant cross sections versus  $x_\perp = 2p_\perp/\sqrt{s}$  at various c.m. energies. The data at  $\sqrt{s} = 23.5, 30.6, 44.8,$  and  $52.7$  GeV are those of Ref. 4 and refer to  $\pi^0$ . The discrepancy between the data at 23.8 and 23.5 GeV should not be considered significant.
- Fig. 4. Particle abundance relative to pions versus  $x_\perp$ .

TABLE CAPTION

Table I. Invariant cross section per nucleon (see text)  $E d\sigma/d^3p$  ( $\text{cm}^2 \text{GeV}^{-2}$ ) for  $\pi^\pm$  mesons produced at  $\sim 90^\circ$  c.m. in p-W collisions, and particle ratios at 200 GeV and 300 GeV incident proton energies. At each  $p_\perp$  value the top line refers to  $\pi^+, K^+/\pi^+, p/\pi^+$ , respectively, and the bottom line to  $\pi^-, K^-/\pi^-, \bar{p}/\pi^-$ . Errors on the cross sections do not include the uncertainty in the absolute calibration.

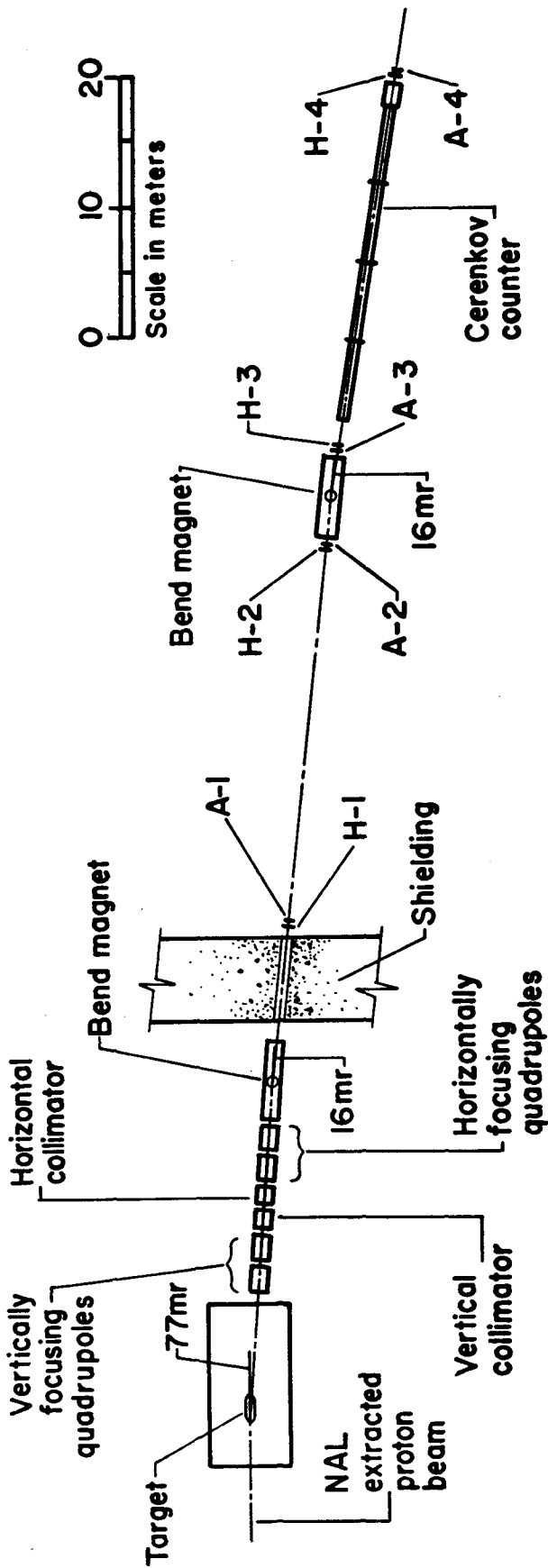


Figure 1

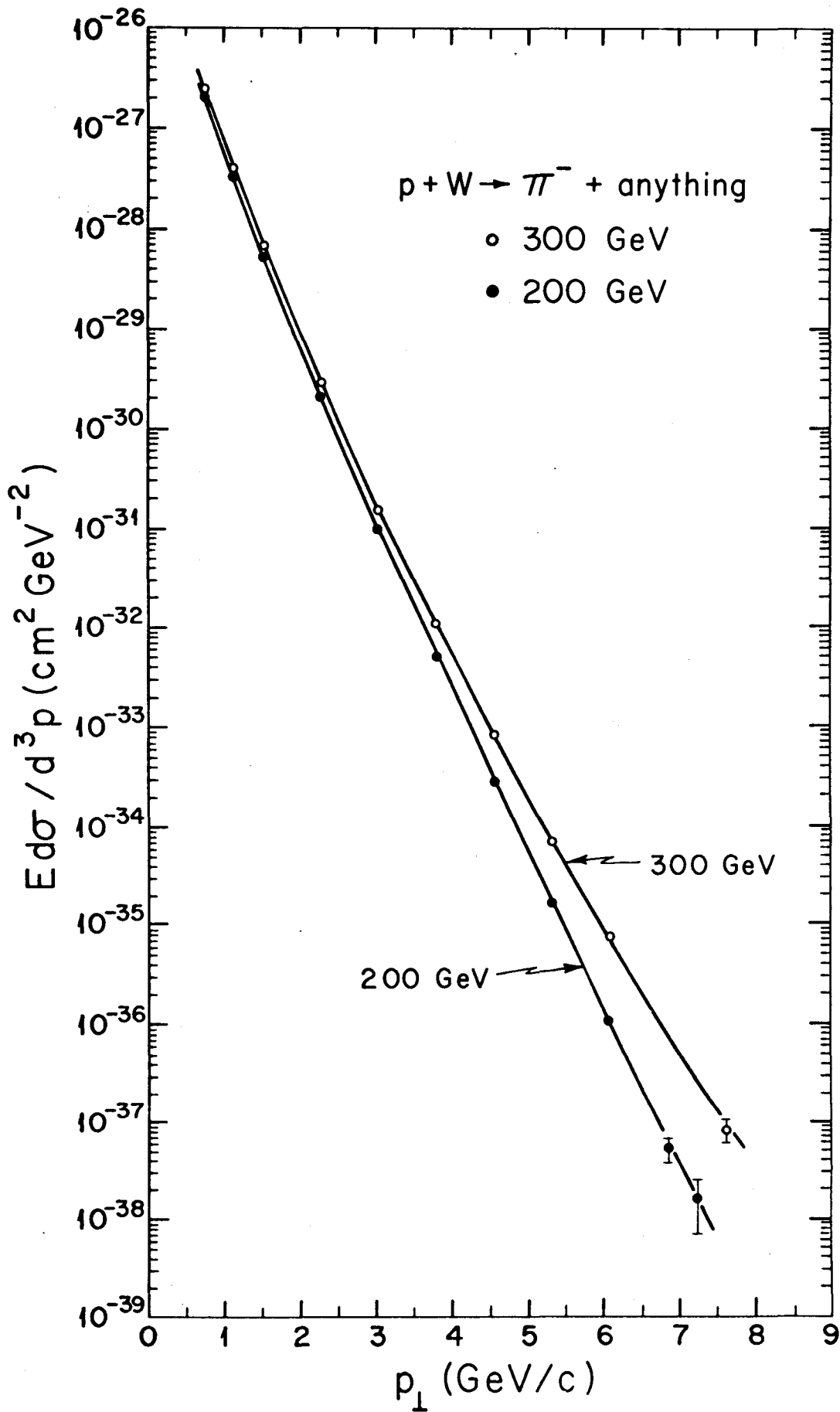


Figure 2

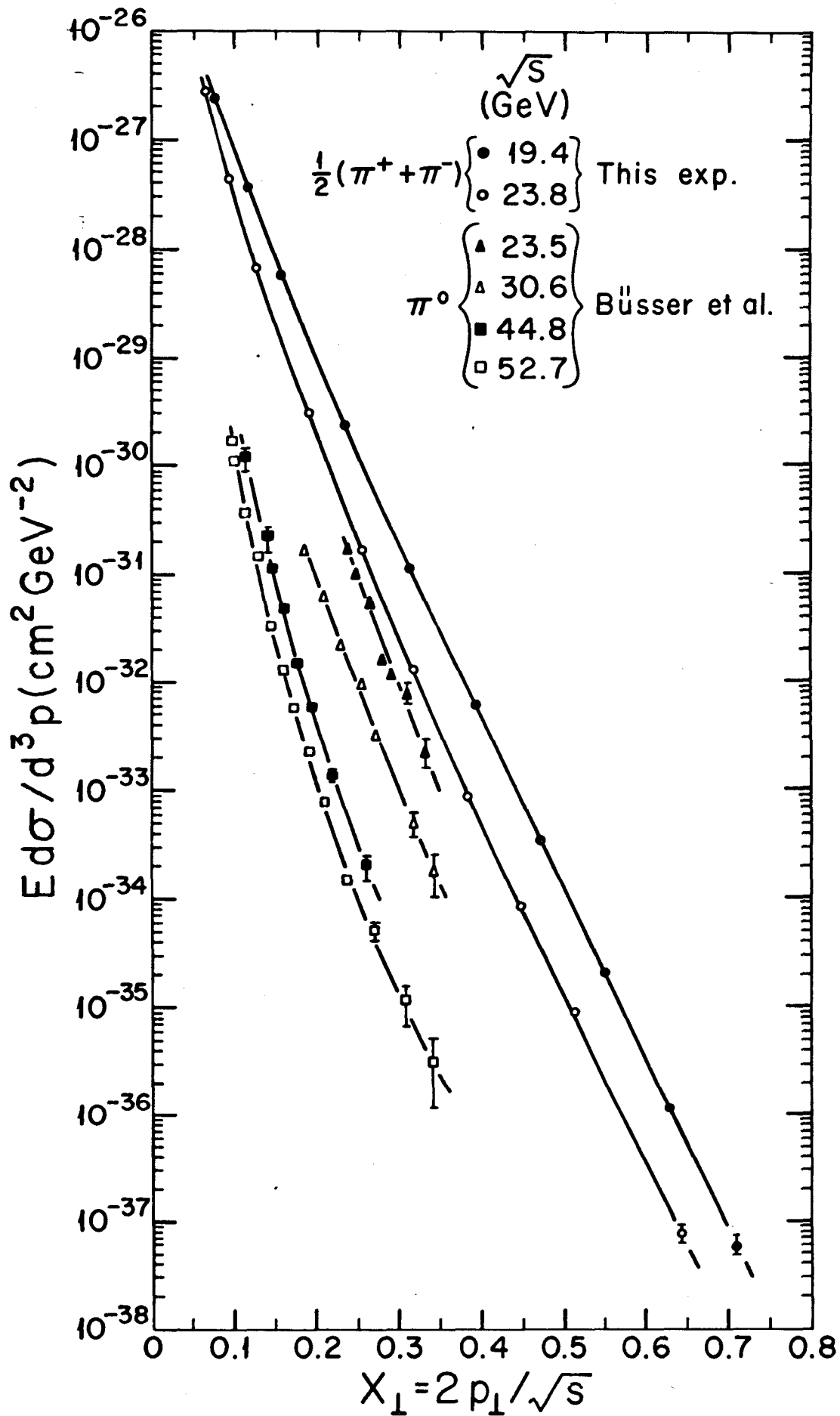


Figure 3

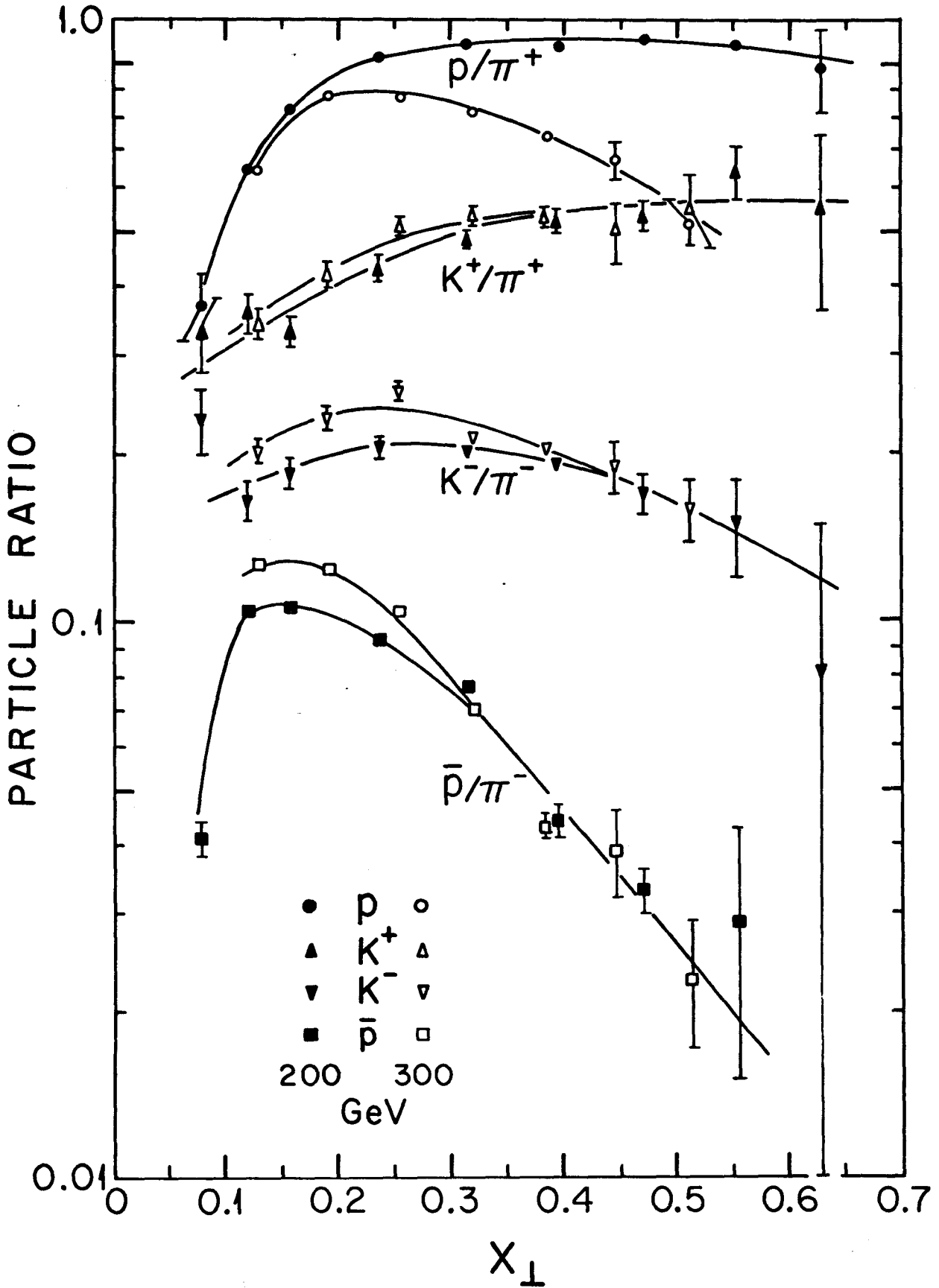


Figure 4

300 GEV

200 GEV

$P_L$ (GeV/c)	$E d\sigma(\pi)/d^3p$	K/ $\pi$	P/ $\pi$	$E d\sigma(\pi)/d^3p$	K/ $\pi$	P/ $\pi$
0.76	(2.69 $\pm$ 0.13) $\times 10^{-27}$ (2.08 $\pm$ 0.10)	0.33 $\pm$ 0.05 0.23 $\pm$ 0.03	0.37 $\pm$ 0.05 0.041 $\pm$ 0.003	(2.89 $\pm$ 0.14) $\times 10^{-27}$ (2.55 $\pm$ 0.13)	0.343 $\pm$ 0.021 0.201 $\pm$ 0.012	0.647 $\pm$ 0.007 0.127 $\pm$ 0.002
1.14	(3.96 $\pm$ 0.20) $\times 10^{-28}$ (3.21 $\pm$ 0.16)	0.358 $\pm$ 0.029 0.165 $\pm$ 0.013	0.646 $\pm$ 0.007 0.104 $\pm$ 0.002	(4.14 $\pm$ 0.21) $\times 10^{-28}$ (4.12 $\pm$ 0.20)	0.421 $\pm$ 0.018 0.231 $\pm$ 0.010	0.871 $\pm$ 0.009 0.124 $\pm$ 0.002
1.53	(6.04 $\pm$ 0.30) $\times 10^{-29}$ (5.31 $\pm$ 0.27)	0.331 $\pm$ 0.020 0.186 $\pm$ 0.011	0.824 $\pm$ 0.009 0.106 $\pm$ 0.002	(6.26 $\pm$ 0.31) $\times 10^{-29}$ (7.07 $\pm$ 0.35)	0.514 $\pm$ 0.015 0.260 $\pm$ 0.008	0.871 $\pm$ 0.004 0.104 $\pm$ 0.001
2.29	(2.56 $\pm$ 0.13) $\times 10^{-30}$ (2.03 $\pm$ 0.10)	0.434 $\pm$ 0.021 0.204 $\pm$ 0.010	1.020 $\pm$ 0.011 0.093 $\pm$ 0.003	(2.95 $\pm$ 0.15) $\times 10^{-30}$ (2.97 $\pm$ 0.15)	0.532 $\pm$ 0.020 0.214 $\pm$ 0.008	0.816 $\pm$ 0.013 0.069 $\pm$ 0.003
3.05	(1.25 $\pm$ 0.06) $\times 10^{-31}$ (0.98 $\pm$ 0.05)	0.485 $\pm$ 0.015 0.201 $\pm$ 0.006	1.093 $\pm$ 0.011 0.076 $\pm$ 0.001	(1.77 $\pm$ 0.09) $\times 10^{-31}$ (1.59 $\pm$ 0.08)	0.531 $\pm$ 0.022 0.205 $\pm$ 0.008	0.742 $\pm$ 0.015 0.043 $\pm$ 0.002
3.81	(6.77 $\pm$ 0.34) $\times 10^{-33}$ (5.01 $\pm$ 0.25)	0.522 $\pm$ 0.024 0.191 $\pm$ 0.007	1.07 $\pm$ 0.02 0.044 $\pm$ 0.003	(1.35 $\pm$ 0.07) $\times 10^{-32}$ (1.14 $\pm$ 0.06)	0.50 $\pm$ 0.06 0.19 $\pm$ 0.02	0.67 $\pm$ 0.05 0.039 $\pm$ 0.007
4.58	(3.86 $\pm$ 0.19) $\times 10^{-34}$ (2.85 $\pm$ 0.14)	0.536 $\pm$ 0.033 0.170 $\pm$ 0.014	1.11 $\pm$ 0.03 0.033 $\pm$ 0.003	(8.78 $\pm$ 0.42) $\times 10^{-34}$ (8.46 $\pm$ 0.46)	0.55 $\pm$ 0.08 0.16 $\pm$ 0.02	0.52 $\pm$ 0.05 0.023 $\pm$ 0.006
5.34	(2.38 $\pm$ 0.12) $\times 10^{-35}$ (1.65 $\pm$ 0.08)	0.64 $\pm$ 0.07 0.15 $\pm$ 0.03	1.09 $\pm$ 0.07 0.029 $\pm$ 0.014	(9.45 $\pm$ 0.57) $\times 10^{-35}$ (6.99 $\pm$ 0.34)		
6.10	(1.30 $\pm$ 0.19) $\times 10^{-36}$ (1.06 $\pm$ 0.12)	0.55 $\pm$ 0.19 0.08 $\pm$ 0.07	0.98 $\pm$ 0.17 < 0.01	(9.82 $\pm$ 0.61) $\times 10^{-36}$ (7.42 $\pm$ 0.53)		
6.87	(6.6 $\pm$ 1.7) $\times 10^{-38}$ (5.2 $\pm$ 1.6)					
7.25	(1.6 $\pm$ 0.9) $\times 10^{-38}$			(6.9 $\pm$ 2.0) $\times 10^{-38}$ (8.1 $\pm$ 2.1)		
7.63						

Table I